Biomechanics in the Inner Ear

Hiroshi Wada

Professor
Department of Bioengineering and Robotics, Graduate School of Engineering
E-mail: wada@cc.mech.tohoku.ac.jp

Abstract

The elongation and contraction of outer hair cells (OHCs) greatly contribute to the high sensitivity and frequency selectivity of the mammalian inner ear. The motility of OHCs is believed to be based on the conformational changes of the motor protein prestin in the plasma membrane of OHCs. In the present study, four lines of research on the inner ear were conducted. First, the mechanism by which the inner ear is protected from acoustic trauma by heat stress was investigated, results showing that such conditioning makes OHCs stiffer, thus enabling them to withstand traumatic noise exposure. Second, imaging of prestin in the plasma membrane of Chinese hamster ovary (CHO) cells was performed by atomic force microscopy (AFM). Results showed that particle-like structures with a diameter of 8–12 nm observed in the CHO plasma membranes were possibly prestin. Third, mutational analysis of prestin was conducted. Consequently, the GTSRH sequence at position 127-131 of the amino acid sequence of prestin was shown to be important for glycosylation and the anion transport function of prestin. Fourth, purification of prestin from prestin-expressing CHO cells was attempted. Results indicate that 120 μg of purified prestin can be obtained from 2×10^9 CHO cells.

1. Introduction

The OHCs in the mammalian cochlea exhibit elongation and contraction in response to acoustical stimulation [1]. This OHC motility results in cochlear amplification, leading to the high sensitivity and sharp frequency selectivity of the mammalian cochlea (Fig. 1). The source of such motility is believed to be conformational changes of the motor protein prestin, densely embedded in the plasma membrane of OHCs.

The impairment of OHCs in the cochlea results in severe hearing loss. Recently, OHCs have been reported to be protected from traumatic exposure by prior sublethal conditioning, such as nontraumatic sound exposure, heat stress, etc. [2]. However, the mechanisms underlying conditioning-related cochlear protection remain unknown.

Prestin has been intensively researched since its identification [3]. By mutational analysis and electron microscopy, its characteristics have been partially clarified. However, the detailed structure of prestin and the mechanism of its conformational change remain unknown.

In the present study, first, to determine the effects of heat stress on the structure of OHCs, Young's modulus of OHCs, which indicates the elasticity of materials and is a factor determining stiffness, and the amount of filamentous actin (F-actin) in OHCs, which is a primary component of the cell cytoskeletal structure, and the expression level of heat shock protein 27 (HSP27) in the cochlea, which is known as a regulator of F-actin polymerization, were measured before and after heat stress by atomic force microscopy (AFM), confocal laser scanning microscopy (CLSM) and Western blotting, respectively. In addition, to evaluate the effects of heat stress on the function of OHCs, distortion product otoacoustic emissions (DPOAEs) and the amount of prestin in OHCs were evaluated before and after heat stress by an ER-10C acoustic system and CLSM, respectively.

Second, to elucidate the structure of prestin, the plasma membrane of CHO cells which express prestin was isolated and then observed by AFM.

Third, to clarify the mechanism of the conformational changes of prestin, an attempt was made to identify the amino acids which play important roles in prestin. Several mutations were introduced into prestin and the characteristics of prestin mutants were then compared with those of wild-type (WT)

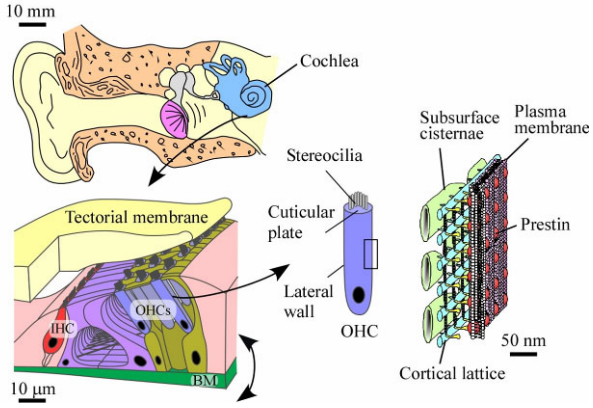

Fig. 1. Human auditory system. Sensory cells, such as outer hair cells (OHCs), inner hair cells and various kinds of the other cells, sit on the basilar membrane (BM). OHCs subject the membrane to force, leading to cochlear amplification, resulting in the high sensitivity of mammalian hearing. Prestin is thought to be the origin of the motility of OHCs.

prestin by patch-clamp recording and Western blotting. Based on the results of the comparison, the roles of mutated amino acids in prestin were examined.

Fourth, for crystal structural analysis of prestin, prestin was extracted and purified from stable prestin-transfected CHO cells. The degree of purification and the amount of purified prestin were then investigated by SDS-PAGE.

2. Mechanism of Inner Ear Protection from Acoustic Trauma by Heat Stress

2.1. Materials and methods

CBA/JNCrj strain male mice, aged 10–12 weeks (25–30 g), were used. The animals were anesthetized and placed in an aluminum boat floating in a hot water bath (46.5°C) to raise their rectal temperature up to 41.5°C. It was maintained at that temperature for 15 min. The animals were then transferred from the boat to a heating pad to fully recover from the anesthesia before being returned to the animal care facility.

To measure Young's modulus of OHCs, the cochleae were detached from the animals in tissue culture medium 3, 6, 12, 24 and 48 h after 15-min heat stress. OHCs were isolated by triturating the organ of Corti in another tissue culture medium. An indentation test was then performed using an AFM (NVB100, Olympus) [4].

For investigation of F-actin of OHCs, the cochleae were detached 3, 6, 12, 24, 48 and 96 h after 15-min heat stress. The organ of Corti was dissected and fixed with 4% paraformaldehyde and then stained with 0.3 μM rhodamine-phalloidin. The images of 16 OHCs obtained at the OHC lateral wall using a CLSM (FV500, Olympus) were subjected to intensity analysis.

DPOAEs were measured using an ER-10C (Etymotic Research) acoustic system. The primary frequency ratio f_2/f_1 was kept constant at 1.20. The stimulus level of f_1 was varied from 20 to 70 dB SPL with steps of 5 dB SPL, while the stimulus level of f_2 was always 10 dB less than that of f_1. DPOAEs were measured at f_2 = 9.8 kHz.

To measure the expression level of HSP27 in the cochlea, the cochleae were detached 6 h after 15-min heat stress. The cochleae were kept in an Eppendorf tube containing 30 μl of lysis buffer (1% Nonidet P-40 non-ionic detergent, 100 μg/ml of phenylmethylsulfonyl fluoride and a 1:50 dilution of proteases inhibitor) and homogenized by sonication in ice. After 1-h lysis, samples were centrifuged at 2,900 × *g* at 4ºC for 10 min and the supernatant was used as the cochlear sample. HSP27 expression was then analyzed by Western blotting.

For investigation of prestin expression in OHCs, they were washed and dehydrated with ethanol after the cochleae were fixed with 4% paraformaldehyde. The cochleae were dissected and the modiolus was exposed. The specimens were then immersed in 0.5% Triton X-100 and the apical turn of the organ of Corti was removed. The specimens were then incubated in 4 μg/ml of goat anti-prestin (C-16) antibody and 4 μg/ml of fluorescein isothiocyanate (FITC) conjugated donkey anti-goat IgG.

2.2. Results

As shown in Fig. 2, the mean and standard deviation of Young's modulus of OHCs in the control group (n = 10) and of those in the anesthesia + heat groups with 3-h (n = 13), 6-h (n = 5), 12-h (n = 8), 24-h (n = 7) and 48-h (n = 12) intervals were 2.1 ± 0.5 kPa, 2.8 ± 0.8 kPa, 2.9 ± 0.6 kPa, 2.7 ± 1.0 kPa, 2.0 ± 0.3 kPa and 2.4 ± 0.6 kPa, respectively. Statistical analysis indicated

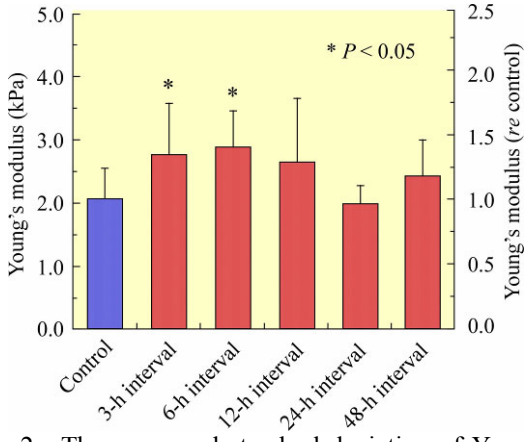

Fig. 2. The mean and standard deviation of Young's moduli of the apical-turn OHCs in the control group (n = 10) and the anesthesia + heat groups with 3-h (n = 13), 6-h (n = 5), 12-h (n = 8), 24-h (n = 7) and 48-h (n = 12) intervals. Statistical analysis indicated significant differences between the control group and the anesthesia + heat groups with 3-h and 6-h intervals, as shown by asterisks (P < 0.05 by Student's t-test).

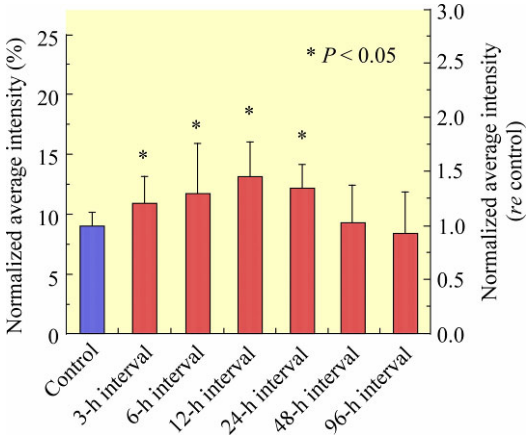

Fig. 3. The mean and standard deviation of the normalized average intensities of F-actin labeling in the control group (n = 25) and the anesthesia + heat groups with 3-h (n = 10), 6-h (n = 19), 12-h (n = 6), 24-h (n = 10), 48-h (n = 10) and 96-h (n = 8) intervals. Asterisks indicate statistically significant differences between the control group and the anesthesia + heat groups (P < 0.05 by Student's t-test).

significant differences between the control group and anesthesia + heat groups with the two shortest intervals, i.e., 3-h and 6-h intervals ($P < 0.05$ by Student's *t*-test). Young's modulus of the mouse OHCs increased by 3 h after heat stress and reached a peak at 6 h, and then began to decrease 12 h after such stress, at which point it was still greater than that of the control group. Young's modulus returned to the pre-conditioning level by 24 h.

Figure 3 shows the mean intensities of F-actin labeling at the lateral wall of OHCs obtained for the control group ($n = 13$) and the anesthesia + heat groups with 3-h ($n = 10$), 6-h ($n = 8$), 12-h ($n = 6$), 24-h ($n = 10$), 48-h ($n = 10$) and 96-h ($n = 8$) intervals. The mean intensity of F-actin increased by 3 h after heat stress, reached a peak at 12 h and then returned to the pre-conditioning level by 24–96 h. Since such intensity is proportional to the amount of a fluorescent substance specifically conjugated with the specimens when the preparation and the observation are performed at the same condition, the intensity of F-actin labeling indicates the amount of F-actin.

Figure 4 shows DPOAE response measured at $f_2 = 9.8$ kHz before ($n = 3$) and 3 h after heat stress ($n = 5$). DPOAE amplitudes 3 h after heat stress were enhanced with statistical significance ($P < 0.05$ by two-way ANOVA).

Figure 5(a) shows an example of the result of HSP27 expression within the cochlea examined by Western blotting. A band is visible at around 27 kDa. Figure 5(b) shows the mean and standard deviation of the normalized intensity of the HSP27 band obtained for the control group ($n = 14$) and the anesthesia + heat group with a 6-h interval ($n = 14$). The intensity of this band increased 1.53-fold by 6 h after heat stress. A significant difference was found between the control and anesthesia + heat groups ($P < 0.05$ by Student's *t*-test).

Figure 6 shows the mean and standard deviation of prestin labeling in the control and anesthesia + heat groups. Significant differences were not found between the control and anesthesia + heat groups with any intervals ($P > 0.05$ by Student's *t*-test).

2.3. Discussion

2.3.1. Effects of heat stress on structure of OHCs

To clarify how the structure of OHCs is modified due to conditioning, Young's modulus and the amount of F-actin of OHCs in the mouse cochlea were investigated in parallel before and after conditioning with heat stress. As shown in Fig. 3, the amount of F-actin increased by 12 h and started to decrease at 24 h. The increase in Young's modulus of OHCs at 3–6 h after heat stress and its decrease at 24–48 h (Fig. 2) showed tendencies similar to those observed in F-actin labeling of the OHC lateral wall. These results suggest that an increase of F-actin due to heat stress

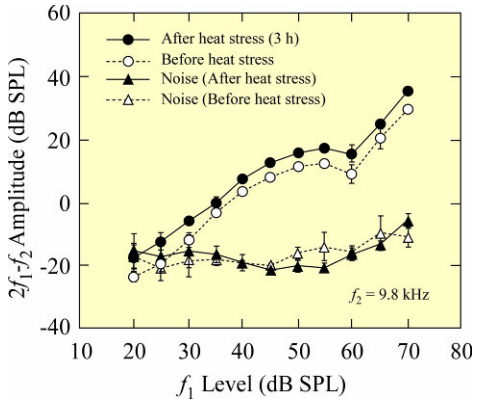

Fig. 4. DPOAE amplitude as a function of the stimulus level of f_1. DPOAE amplitudes 3 h after heat stress at $f_2 = 9.8$ kHz were enhanced with statistical significance ($P < 0.05$ by two-way ANOVA).

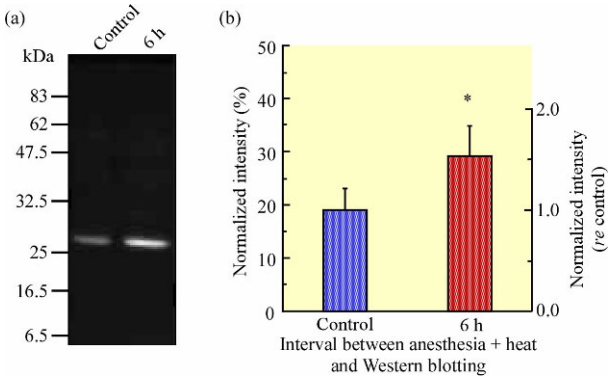

Fig. 5. Expression of HSP27 in the mouse cochlea. (a) An example of Western blotting. (b) The mean intensity of the normalized intensity of the HSP 27 band in the control group ($n = 14$) and the anesthesia + heat group ($n = 14$). The asterisk indicates a statistically significant difference between the control group and the anesthesia + heat group ($P < 0.05$, Student's *t*-test).

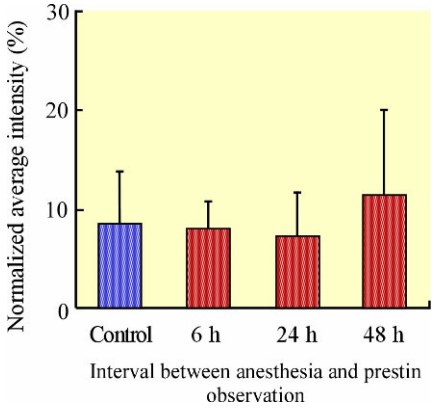

Fig. 6. The mean and standard deviation of the normalized average intensities of prestin labeling in the control group ($n = 18$) and the anesthesia + heat groups with 6-h ($n = 10$), 24-h ($n = 11$) and 48-h ($n = 10$) intervals. Statistically significant differences between the control group and the anesthesia + heat groups with any intervals were not found ($P > 0.05$, Student's *t*-test).

presumably leads to an increase of Young's modulus of OHCs since F-actin is a primary component of the cytoskeleton of OHCs which contributes the mechanical properties of the cells, rendering the cells stiffer, resulting in protection of mammalian hearing from subsequent traumatic exposure.

Although the exact mechanism of the increase of F-actin due to heat stress is unclear, the regulation of HSPs is a likely candidate as a source of such increase. Among such HSPs, HSP27 is known as a regulator of F-actin polymerization, which acts as a barbed-end F-actin capping protein and inhibits actin polymerization. However, heat stress induces rapid phosphorylation of pre-existing HSP27 and leads to a loss of its actin capping activity [5], resulting in an acceleration of actin polymerization. As shown in Fig. 5, the expression level of HSP27 in the cochlea was confirmed to increase 6 h after heat stress. The expression and localization of HSP27 have been previously confirmed at the cuticular plate and the lateral walls of OHCs [6]. In the present study, therefore, the polymerization of F-actin in OHCs may possibly have been accelerated by increasing the expression level of HSP27 after conditioning with heat stress and caused the amount of F-actin in OHCs to increase, thereby leading to an increase in Young's modulus of OHCs.

2.3.2. Effects of heat stress on function of OHCs

To explore how the function of OHCs is modified due to conditioning, DPOAEs were measured before and after conditioning with heat stress. We confirmed the statistically significant enhancement of DPOAEs 3 h after heat stress at f_2 = 9.8 kHz (Fig. 4). The enhancement of DPOAEs is probably due to functional change of OHCs since DPOAEs substantially rely on the electromotility of OHCs.

By considering a possible generation mechanism of DPOAEs using an equivalent mechanical model of the organ of Corti, a relationship between the heat stress-induced increase in the stiffness of OHCs and an enhancement of DPOAE amplitude can be explained. If we make a simplifying assumption based on these reports, the basilar membrane (BM) can be likened to a spring with a stiffness of k_{BM} and the reticular lamina (RL) can be expressed as a rigid wall since it is undeformable. Regarding the OHC, it can be represented as a series of a displacement generator (DG), i.e., the motor protein prestin, and a spring indicating the stiffness of the OHC, k_{OHC}, as previously reported [7–9]. An equivalent mechanical model of the organ of Corti was constructed by a series of those three components, as shown in Fig. 7. Based on this model, when the DG deforms x_1, the force generated by the OHC, F, is given by

$$F = \frac{k_{OHC}k_{BM}}{k_{OHC}+k_{BM}}x_1 = \frac{k_{BM}}{1+\frac{k_{BM}}{k_{OHC}}}x_1 \quad (1)$$

According to Hooke's law, displacement of the BM, x_2, is given by

$$x_2 = \frac{F}{k_{BM}} \quad (2)$$

Assuming a cylindrical shape and homogeneity of the OHC, the stiffness of the OHC, k_{OHC}, is proportional to its Young's modulus. An increase in Young's modulus of OHCs therefore results in an increase in the stiffness of OHCs, k_{OHC}. Derived from Eq. (1), greater stiffness of OHCs, k_{OHC}, results in greater force generated by OHC, F. Consequently, the displacement of the BM, x_2, is amplified (Eq. (2)), leading to an enhancement of DPOAE amplitude.

In our previous study, DPOAE amplitude was found to be enhanced with statistical significance after heat stress [10]. DPOAE amplitude has been reported to be concerned with the amount of prestin. In a report on prestin knockout mice, DPOAE thresholds of homozygous mice (-/-), which did not express the prestin gene and protein, were higher than those of wild type mice [11]. In addition, 2-week administration of salicylate in guinea pigs has been reported to enhance DPOAE amplitude [12] as well as to enhance prestin mRNA expression [13], suggesting that the high level expression of prestin induced by salicylate results in the enhancement of DPOAE amplitude. These results indicate that there is a possibility that the

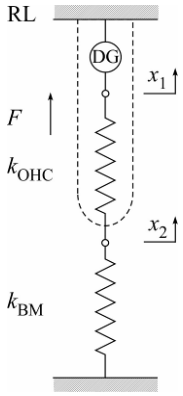

Fig. 7. Equivalent mechanical model of the organ of Corti. The organ of Corti was expressed as a series consisting of the reticular lamina (RL), which was expressed as a rigid wall since it is undeformable, the OHC, which was represented by a series of a displacement generator (DG), i.e., the motor protein prestin, and a spring indicating the OHC stiffness, k_{OHC}, and the basilar membrane (BM), which was shown as a spring with a stiffness of k_{BM} [7-9]. When the DG deforms x_1, the OHC subject the BM to force, F, leading to a certain amount of displacement of the BM, x_2.

amount of prestin in OHCs increases after heat stress. However, in the present study, we found that the amount of prestin did not change after heat stress. Thus, the DPOAE enhancement demonstrated in our previous study is thought to be induced by a prestin-independent pathway. Instead, this enhancement is induced by the increase in OHC stiffness, as reported in our previous study [10].

3. Visualization by AFM of the Motor Protein Prestin

3.1. Materials and methods

Experiments were performed in prestin-transfected CHO cells [14] and untransfected CHO cells. Cells were cultured in RPMI-1640 medium with 10% fetal bovine serum, 100 U penicillin/ml and 100 μg streptomycin/ml at 37°C with 5% CO_2. The cells were collected by centrifugation at 250 × *g* for 5 min and the supernatant was removed. The cells were then agitated with an external solution (140 mM KCl, 3.5 mM $MgCl_2$, 5 mM EGTA, 5 mM HEPES and 0.1 mM $CaCl_2$; pH 7.3) and deposited on plastic dishes. After ten minutes, these cells were sonicated in a hypotonic buffer (10 mM PIPES, 10 mM $MgCl_2$, 0.5 mM EGTA; pH 7.2). The membranes attached to the substrate were then incubated with a high salt buffer (2 M NaCl, 2.7 mM KCl, 1.5 mM KH_2PO_4, 1 mM Na_2HPO_4; pH 7.2) and 0.05% trypsin to remove the cytoskeletal materials and the peripheral membrane proteins. The membranes were fixed with 1% glutaraldehyde and then incubated with 2 mM CM-DiI. Finally, the membranes were immersed in filtered 0.1 M phosphate buffer solution.

The AFM system (NVB100, Olympus) used for the experiments consists of a cantilever, laser, mirror, photodiode array, feedback system and piezoscanner. A V-shaped silicon nitride cantilever (OMCL-TR400PSA-2, Olympus) with a spring constant of 0.02 N/m was used. The typical radius of curvature of the cantilever tip was 16 nm. To reduce sample damage during scanning, images were obtained using the oscillation mode (Tapping mode™, Digital Instruments, Santa Barbara, CA). The cantilever was oscillated near its resonance frequency in liquid (3.6–4.7 kHz). High-magnification images (scan size is 1.0 × 0.5 μm) were obtained from the isolated membranes of the prestin-transfected CHO cells and those of the untransfected CHO cells. The scan speed is 0.3–0.4 μm/s.

The original AFM images were flattened by use of a software program (Digital Instruments, Santa Barbara, CA) to eliminate background slopes and to correct dispersions of individual scanning lines. In this study, differential images were computed from the original flattened AFM images for further analysis of the imaged structures by using Adobe Photoshop 6.0. First, the colored original flattened AFM images were converted into gray-scale AFM images. To remove the noise of the images, spatial averaging was then performed at each pixel of the images. After averaging, differential operation was performed by a command "find edges." For analysis of the diameters of the observed structures, a simple geometric model, as shown in Fig. 8, was used since such sizes are prone to overestimation due to the radius of the curvature of the AFM tip [15]. When the observed structure was regarded as a sphere in the plasma membrane, the relationship between the diameter of the structure observed by the AFM (2Δ) and its actual diameter ($2r$) is given by

$$2\Delta = 2\sqrt{(R+r)^2 - (R+H/2)^2} \tag{3}$$

where R and H are the radius of the curvature of the AFM tip and the thickness of the plasma membrane, respectively. The former is 16 ± 1 nm and the latter is 5 nm in the present measurements.

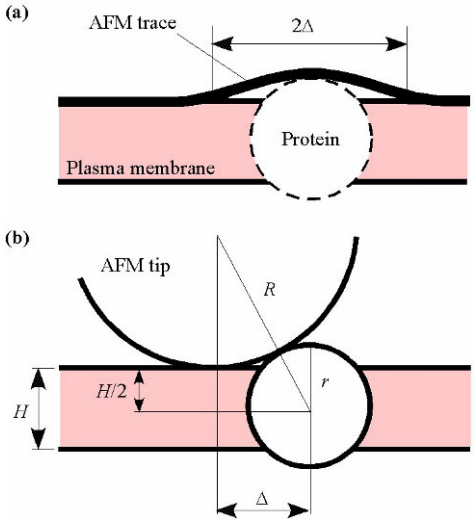

Fig. 8. A sphere model of a membrane protein. (a) AFM trace. (b) Geometric relationship between the AFM tip and a membrane protein. Due to the curvature of the AFM tip, the lateral dimensions of the image are overestimated.

3.2. Results

Figure 9 represents three-dimensional AFM images of the isolated plasma membranes of the prestin-transfected and untransfected CHO cells. Particle-like structures were recognized in the plasma membranes of both cells; however, no distinctive difference in such particle-like structures was found between these cells.

In this study, when the size of the particle-like structures was over 100 nm, they were neglected because the size of the membrane proteins is on the order of tens of nanometers. When the shape index, i.e., the ratio of the minor axis length to the major axis length, was 0.5–1.0, the structure was regarded as being a particle-like structure.

Since there are many kinds of membrane proteins in the plasma membrane of CHO cells, it is impossible to

clarify whether the observed structures are prestin or not. Analysis of the shape and size of the observed structures was therefore performed for five AFM images of the prestin-transfected CHO cells and five such images of the untransfected CHO cells. The frequency distribution of the observed particle-like structures, i.e., the density of the particle-like structuresplotted against diameter of those structures with 2-nm intervals, is shown in Fig. 10. The diameters of the particle-like structures of the prestin-transfected CHO cells ranged from 6 to 40 nm, and those of the untransfected CHO cells ranged from 6 to 30 nm. When the sizes of the particle-like structures in the plasma membranes were 8–10 nm and 10–12 nm, the differences of their densities between the prestin-transfected CHO cells and the untransfected CHO cells were statistically significant for $P < 0.05$ using Student's t-test, as indicated by asterisks.

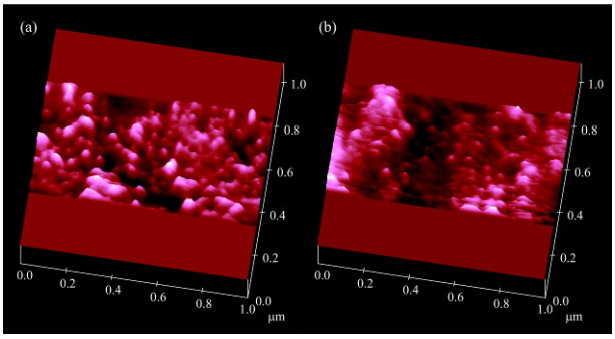

Fig. 9. Three-dimensional AFM images of the isolated plasma membranes of the CHO cells. (a) Prestin-transfected CHO cell. (b) Untransfected CHO cell. More particle-like structures with a diameter of 8–12 nm exist in the plasma membrane of the prestin-transfected CHO cells than in that of the untransfected CHO cells.

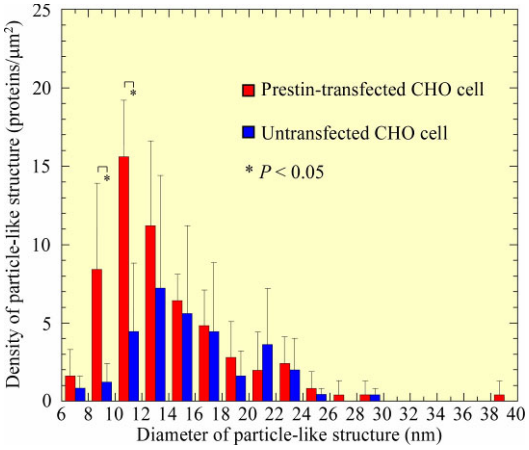

Fig. 10. Frequency distribution of the observed particle-like structures in the plasma membrane. The density of the particle-like structure is plotted against the interval in 2-nm classes. Data were obtained from five AFM images of the prestin-transfected CHO cells and five such images of the untransfected CHO cells. When the sizes of the particle-like structures were 8–10 nm and 10–12 nm, differences of their densities between the prestin-expressing CHO cells and the untransfected CHO cells were statistically significant for $P < 0.05$ using Student's *t*-test, as shown by the asterisks. Error bars represent standard deviations.

3.3. Discussion

In this study, to obtain isolated plasma membranes, the cells were sheared open by sonication and the cytoplasmic surfaces were exposed. However, cytoskeletal materials and peripheral proteins may remain on the cytoplasmic surface with such treatment. Such residue is thought to obstruct observation of the membrane proteins. To remove these materials, incubation of isolated plasma membranes with the high salt buffer and trypsin was performed. As the structure of prestin is not degraded and deformed by trypsin [14], the prepared sample is expected to be suitable for the experiment using AFM.

Since the difference between the prestin-transfected and untransfected CHO cells is due to the existence of prestin, the difference of the densities of the particle-like structures between the prestin-expressing CHO cells and the untransfected CHO cells is considered to be caused by the presence or absence of prestin. Based on Fig. 10, therefore, the majority of these particle-like structures with a diameter of 8–12 nm in the prestin-transfected CHO plasma membrane are possibly prestin. This result is consistent with the expected diameter of prestin (~7 nm in diameter) based on its molecular weight.

4. Mutational Analysis of the Motor Protein Prestin

4.1. Methods and methods

The present study focused on the GTSRH seqeuence at position of 127-131 of an amino acid sequence of prestin (Fig. 11). The GTSRH sequence was altered, i.e., alanine (A) was substituted for glycine, threonine, serine, arginine and histidine individually and threonine was substituted for serine, resulting in six prestin mutants, namely, G127A, T128A, S129A, R130A, H131A and S129T. Wild-type prestin and the prestin mutants were expressed in human embryonic kidney (HEK) 293 cells. Moreover, FLAG-tagged WT prestin and FLAG-tagged prestin mutants were expressed in HEK293 cells for Western blotting.

To confirm the expression of FLAG-tagged prestin mutants and the molecular weight of the expressed proteins, Western blotting was performed using anti-FLAG antibody. By comparing the positions of a protein maker and that of detected band, the molecular weight of the expressed proteins were examined. Functional analysis of the prestin mutants were conducted by the whole-cell patch-clamp recording. WT prestin-expressing cells exhibit bell-shaped nonlinear capacitance (NLC) in response to the change of membrane potential. The anion transport function of

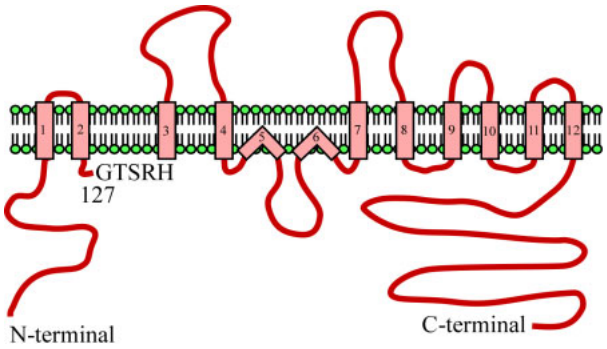

Fig. 11. Putative topology model of prestin [17]. The GTSRH sequence of amino acids at positions 127-131 was completely conserved in six proteins of the SLC26A family.

prestin was generally evaluated with NLC. NLC is well fitted to the derivative of a Boltzman function,

$$C_{\mathrm{m}}(V) = C_{\mathrm{lin}} + \frac{Q_{\max}}{\alpha \mathrm{e}^{\frac{V-V_{1/2}}{\alpha}} \left(1+\mathrm{e}^{-\frac{V-V_{1/2}}{\alpha}}\right)^2} \quad (4)$$

where C_{lin} is linear capacitance, $Q_{\max}$ is maximum charge transfer, V is membrane potential, $V_{1/2}$ is the voltage at which the maximum charge is equally distributed across the membrane and α is the slope factor of voltage dependence of charge transfer.

To estimate the NLC of unit cell surface, the normalized NLC $C_{\mathrm{nonlin/lin}}$ was defined as

$$C_{\mathrm{nonlin/lin}}(V) = \frac{C_{\mathrm{nonlin}}}{C_{\mathrm{lin}}} = \frac{\left(C_{\mathrm{m}}(V) - C_{\mathrm{lin}}\right)}{C_{\mathrm{lin}}} \quad (5)$$

where C_{nonlin} is the nonlinear component of the measured membrane capacitance. Furthermore, to compare the normalized data of the point mutants with that of the WT prestin, C_{nonlin} (V) was divided by the maximum $C_{\mathrm{nonlin}}(V)$ of WT prestin and termed relative C_{nonlin} (V).

4.2. Result

The results of Western blotting of HEK293 cells separately transfected with an empty vector, WT prestin or the prestin mutants are shown in Fig. 12. The theoretical molecular weights of FLAG-tagged WT prestin and FLAG-tagged prestin mutants are 84.6 kDa. Two major bands of about 100 kDa and 70 kDa were detected in WT prestin. One major band of about 80 kDa was detected in FLAG-tagged prestin mutants.

Relative C_{nonlin} (V) plots are shown in Fig. 13. WT prestin (n = 20), G127A (n = 10), T128A (n = 10), S129A (n = 10) and R130A (n = 11) exhibited the NLC versus membrane potential. However, the maximum relative C_{nonlin} (V) of these mutants was significantly smaller than that of WT prestin. On the other hand, the membrane capacitance of cells transfected with H131A (n = 11) or S129T (n = 10) versus membrane potential was constant, similar to the data from the cells transfected with the empty vector.

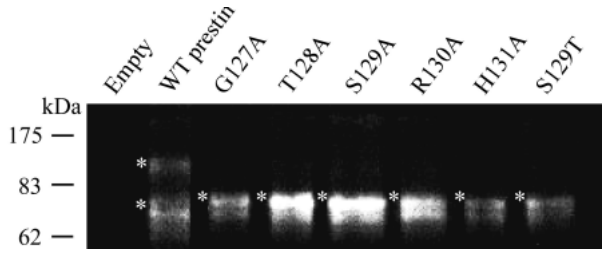

Fig. 12. Result of Western blotting. Major bands are indicated by asterisks. There was no band in the empty vector. Two major bands of about 100 kDa and 70 kDa were detected in wild-type (WT) prestin. One major band of about 80 kDa was detected in the prestin mutants.

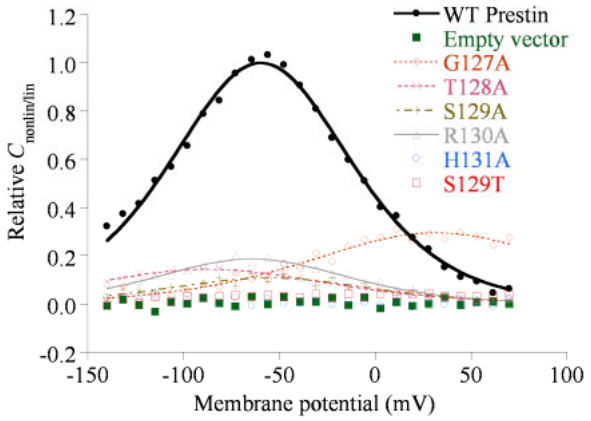

Fig. 13. Results of whole-cell patch-clamp for WT prestin and the prestin mutants. WT prestin (n = 20), G127A (n = 10), T128A (n = 10), S129A (n = 10) and R130A (n = 11) exhibited the NLC versus membrane potential. On the other hand, the membrane capacitance of cells expressing H131A (n = 11) or S129T (n = 10) versus membrane potential was constant, similar to the data from the cells transfected with the empty vector.

4.3. Discussion

Taking account of the fact that prestin is a glycoprotein [18], the 100 kDa and 80 kDa bands detected in WT prestin are thought to be glycosylated and unglycosylated prestin, respectively. The molecular mass of the prestin mutant bands was larger than that of the unglycosylated WT prestin band and smaller than that of the glycosylated WT prestin band. Thus, it was considered that although the prestin mutants were glycosylated, there was a difference in glycosylation structure between WT prestin and the prestin mutants.

By the mutations in the GTSRH sequence, NLC significantly decreased or disappeared. NLC represents the anion transport function of prestin in the plasma membrane of transfected cells. Therefore, the decrease or loss of NLC indicates a decrease or loss of the anion transport function of prestin by the mutations. From the results of Western blotting and the patch-clamp recording, it is concluded that the GTSRH sequence is involved in the glycosylation and the anion transport function of prestin.

5. Purification of the Motor Protein Presitn

5.1. Materials and methods

In this study, Chinese hamster ovary (CHO) cells which had been modified to stably express C-terminal 3×FLAG-tagged prestin [12] were used. Generally, membrane proteins require detergents for solubilization. Although there are many kinds of detergents, it is unclear which are suitable to solubilize prestin. In this study, 8 different detergents, commonly used for membrane protein solubilization, i.e., octyl glucoside, dodecyl maltoside , nonyl thiomaltoside , sucrose monocholate , sucrose monocaprate , sucrose monolaurate, MEGA-9, CHAPSO were tested. First, 5×10^6 cells were incubated on ice with 100 μl of 10 mM Hepes buffer (pH 7.3) containing 140 mM NaCl, 5 mM KCl, 1 mM $MgCl_2$, 1.5 mM $CaCl_2$ and the different detergents at various concentrations for 30 min. After the incubation, samples were centrifuged at 20,360 × g at 4ºC for 2 h. Proteins contained in the supernatant and those in the precipitate were defined as solubilized proteins and non-solubilized proteins, respectively. The ratio of prestin in supernatants (solubilized prestin) to that in precipitates (non-solubilized prestin) was analyzed by quantitative Western blotting.

Next, purification of prestin was attempted using the selected detergent. First, 2×10^9 cells expressing 3×FLAG-tagged prestin in 40 ml of 10 mM Hepes buffer (pH 7.3) containing 150 mM Na_2SO_4 were disrupted by sonication, followed by centrifugation at 1,000 × g for 7 min at 4ºC to remove nuclei and undisrupted cells. The supernatant was centrifuged at 20,360 × g at 4ºC for 2 h to separate the cytoplasmic soluble fraction and the membrane fraction. To solubilize membrane proteins, the obtained membrane fraction was resuspended in 40 ml of the same Hepes buffer containing 10 mM nonyl thiomaltoside. This buffer was subsequently used for all procedures. After 2-h incubation on ice, the non-solubilized proteins were removed by centrifugation at 20,360 × g at 4ºC for 2 h. The supernatant, which contained the solubilized prestin, was applied to a column of anti-FLAG affinity gel, prestin tagged with 3×FLAG epitope being expected to bind to the column. After washing the column, bound proteins were competitively eluted with the buffer containing 250 μg/ml of 3×FLAG peptide.

5.2. Results and discussion

The relationship between the detergent concentration and the solubilization efficiency using nonyl thiomaltoside is shown in Fig. 14. Solubilization efficiency sharply increased around the critical micelle concentration (cmc). Since this tendency agrees with those in the previous reports in which target membrane proteins were solubilized with detergents in active form, it is expected that nonyl thiomaltoside may solubilize prestin in active form. The detergent concentration was decided based on a report that it should be close to the saturation points of solubilization efficiency. Since such point for nonyl thiomaltoside in the present study was 10 mM, it was determined that 10 mM nonyl thiomaltoside was applied for prestin purification. The solubilization efficiency was 74%.

Purification of prestin was performed using nonyl tiomaltoside and the anti-FLAG affinity column. The result of sodium dodecyl sulfate-polyacrylamide gel electrophoresis (SDS-PAGE) loaded with obtained purified sample is shown in Fig. 15. A major band around 100 kDa (arrowhead) indicating prestin was detected. The amount of obtained purified prestin was determined by quantitative Western blotting. As a result, it was estimated that about 120 μg of purified prestin was obtained from 2×10^9 3×FLAG-tagged prestin-expressing CHO cells.

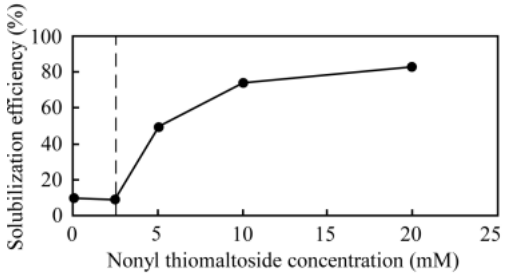

Fig. 14. Relationships between the nonyl thiomaltoside concentration and the solubilization efficiency. The filled circles, connected by solid lines, indicate the solubilization efficiency obtained by quantitative Western blotting. Dashed lines show each critical micelle concentration (cmc).

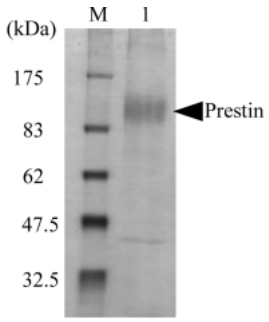

Fig. 15. Silver-stained SDS-PAGE gel loaded with purified prestin. The arrowhead shows prestin. Lane M: molecular weight marker. Lane 1: purified prestin.

6. Conclusions

Analysis of effects of heat stress on the structure and function of OHCs, imaging of prestin by AFM, mutational analysis of prestin and its purification were performed, the results indicating the following:

1. HSP27 in the cochlea increased due to conditioning with heat stress. The amount of F-actin in the lateral wall of OHCs increased after heat stress due to the overexpression of HSP27. In addition, conditioning with heat stress caused an increase in Young's modulus of mouse OHCs at 3–6 h after heat stress. This factor returned to the pre-conditioning level by 24–48 h after heat stress. The increase and decrease in Young's modulus of the OHCs showed tendencies similar to those in the amount of their F-actin. These results suggest that an increase in F-actin of OHCs due to heat stress may possibly lead to an increase their stiffness, resulting in protection of the ear against noise-induced hearing loss. Although DPOAE was found to increase due to heat stress, the amount of prestin at the lateral wall of OHCs did not change. Thus, the DPOAE enhancement is thought to be induced by a prestin-independent pathway. Instead, this enhancement is induced by the increase in OHC stiffness.

2. Membranes of prestin-transfected and untransfected CHO cells were observed by AFM. More particle-like structures with a diameter of 8–12 nm exist in the plasma membrane of the prestin-transfected CHO cells than in that of the untransfected CHO cells. This result suggests that such particle-like structures with a diameter of 8–12 nm are possibly prestin molecules.

3. Mutations in the GTSRH sequence of prestin caused the change in glycosylation pattern of prestin and the decrease in its anion transport function, suggesting that that sequence is involved in glycosylation of prestin and its anion transport function.

4. It was clarified that 10 mM nonyl thiomaltoside is optimum to solubilize prestin. About 120 μg of purified prestin was obtained from 2×10^9 3×FLAG-tagged prestin-expressing CHO cells.

Acknowledgements

Hiroshi Wada acknowledges the support of Tohoku University Global COE Program "Global Nano-Biomedical Engineering Education and Research Network Centre," as well as that of the following grants: Gtrant-in-Aid for Scientific Research on Priority Areas 15086202 from the Ministry of Education, Culture, Sports, Science and Technology of Japan, Grant-in-Aid for Scientific Research (B) 18390455 from the Japan Society for the Promotion of Science, that of Grant-in-Aid for Exploratory Research 18659495 from the Ministry of Education, Culture, Sports, Science and Technology of Japan, the Human Frontier Science Program, a Health and Labour Science Research Grant from the Ministry of Health, Labour and Welfare of Japan, the Iketani Science and Technology Foundation and the Daiwa Securities Health Foundation.

References

[1] Brownell WE, Bader CR, Bertrand D, and de Ribaupierre Y. Evoked mechanical responses of isolated cochlear outer hair cells. *Science* **227**, 194-196, 1985.

[2] Yoshida N, Kristiansen A, and Liberman MC. Heat stress and protection from permanent acoustic injury in mice. *J Neurosci* **19**, 10116–10124, 1999.

[3] Dallos P, Zheng J, and Cheatham MA. Prestin and the cochlear amplifier. *J Physiol* **576**, 37-42, 2006.

[4] Murakoshi M, Yoshida N, Iida K, Kumano S, Kobayashi T, and Wada H. Local mechanical properties of mouse outer hair cells: atomic force microscopic study. *Auris Nasus Larynx* **33**, 149–157, 2006.

[5] Clark JI and Muchowski PJ. Small heat-shock proteins and their potential role in human disease. *Curr Opin Struct Biol* **10**, 52–59, 2000.

[6] Leonova EV, Fairfield DA, Lomax MI, and Altschuler RA. Constitutive expression of Hsp27 in the rat cochlea. *Hear Res* **163**, 61–70, 2002.

[7] Hallworth R. Passive compliance and active force generation in the guinea pig outer hair cell. *J Neurophysiol* **74**, 2319–2328, 1995.

[8] He DZZ and Dallos P. Somatic stiffness of cochlear outer hair cells is voltage-dependent. *Proc Natl Acad Sci USA* **96**, 8223–8228, 1999.

[9] He DZZ and Dallos P. Properties of voltage-dependent somatic stiffness of cochlear outer hair cells. *J Assoc Res Otolaryngol* **1**, 64–81, 2000.

[10] Murakoshi M, Yoshida N, Kitsunai Y, Iida K, Kumano S, Suzuki T, Kobayashi T, and Wada H. Effects of heat stress on Young's modulus of outer hair cells in mice. *Brain Res* **1107**, 121–130, 2006.

[11] Liberman MC, Gao J, He DZZ, Wu X, Jia S, and Zuo J. Prestin is required for electromotility of the outer hair cell and for the cochlear amplifier. *Nature* **419**, 300–304, 2002.

[12] Huang Z-W, Luo Y, Wu Z, Tao Z, Jones RO, and Zhao H-B. Paradoxical enhancement of active cochlear mechanics in long-term administration of salicylate. *J Neurophysiol* **93**, 2053–2061, 2005.

[13] Zhu M-L, Yu N, and Zhao H-B. Upregulation of prestin expression in long-term administration of salicylate. *Assoc Res Otolaryngol* Abs, 373, 2006.

[14] Iida K, Tsumoto K, Ikeda K, Kumagai I, Kobayashi, T, and Wada H. Construction of an expression system for the motor protein prestin in Chinese hamster ovary cells. *Hear Res* **205**, 262-270, 2005.

[15] Larmer J, Schneider SW, Danker T, Schwab A, and Oberleithner H. Imaging excised apical plasma

membrane patches of MDCK cells in physiological conditions with atomic force microscopy. *Pflugers Arch* **434**, 254-260, 1997.
[16] Kakehata S and Santos-Sacchi J. Membrane tension directly shifts voltage dependence of outer hair cell motility and associated gating charge. *Biophys J* **68**, 2190-2197, 1995.
[17] Deák L, Zheng J, Orem A, Du GG, Aguiñaga S, Matsuda K, and Dallos P. Effects of cyclic nucleotides on the function of prestin. *J Physiol* **563**, 483-496, 2005.
[18] Matsuda K, Zheng J, Du GG, Klöcker N, Madison LD, and Dallos P. N-Linked glycosylation sites of the motor protein prestin: effects on membrane targeting and electrophysiological function. *J Neurochem* **89**, 928-938, 2004.